Strain-rate dependent properties of short carbon-fiber reinforced Acrylonitrile-Butadiene-Styrene using Material Extrusion Additive Manufacturing

Wilco M.H. Verbeeten[a,*], Miriam Lorenzo-Bañuelos[a], Rubén Saiz-Ortiz[b,c], Rodrigo González[c]

[a]*Structural Integrity Research Group, Universidad de Burgos, Avenida Cantabria s/n, E-09006, Burgos, Spain*
[b]*Escuela Politécnica Superior, Universidad de Burgos, Avenida Cantabria s/n, E-09006, Burgos, Spain*
[c]*Benteler España SAU, Calle López Bravo 57, E-09001, Burgos, Spain*

Abstract

Purpose - The objective of the present paper is to quantify and analyze the strain-rate dependence of the yield stress for both unfilled Acrylonitrile-Butadiene-Styrene (ABS) and short carbon-fiber reinforced ABS (CF-ABS) materials, fabricated via material extrusion additive manufacturing (ME-AM). Two distinct and opposite infill orientation angle were used to attain anisotropy effects.

Design/methodology/approach - Tensile test samples were printed with two different infill orientation angles. Uniaxial tensile tests were performed at 5 different constant linear strain rates. Apparent densities were measured to compensate for the voided structure. SEM fractography images were analyzed. An Eyring-type flow rule was evaluated for predicting the strain-rate dependent yield stress.

Findings - Anisotropy was detected not only for the yield stresses, but also for its strain-rate dependence. The short carbon-fiber filled material exhibited higher anisotropy than neat ABS material using the same ME-AM processing parameters. It seems that fiber and molecular orientation influence the strain-rate dependence. The Eyring-type flow rule can adequately describe the yield kinetics of ME-AM components, showing thermorheologically simple behavior.

Originality/value - A polymer's viscoelastic behavior is paramount to be able to pre-

*Corresponding author
Email address: wverbeeten@ubu.es (Wilco M.H. Verbeeten)

dict a component's ultimate failure behavior. The results in this manuscript are important initial findings that can help to further develop predictive numerical tools for ME-AM technology. This is especially relevant due to the inherent anisotropy that ME-AM polymer components show. Furthermore, short carbon-fiber filled ABS enhanced anisotropy effects during ME-AM, which has not been measured previously.

Keywords: Fused Filament Fabrication (FFF); Polymer-matrix composites (PMC); ABS material; Infill orientation; Anisotropic strain-rate dependent yield stress; Eyring rate equation; Apparent density.

Paper type Research paper

---

1. Introduction

Material Extrusion Additive Manufacturing (ME-AM) (ISO/ASTM 52900, 2015), also known as Fused Deposition Modeling (FDM ®), Fused Filament Fabrication (FFF), Fused Layer Modeling (FLM), or 3D printing, is one of the most widely used freeform fabrication techniques for polymer components. It is mainly employed for Rapid Prototyping (RP), although the technique is increasingly used for Rapid Manufacturing (RM) as well. Its popularity derives from a combination of low investment costs and an ease for the fabrication of customized end-use products with a variety of materials (Turner *et al.*, 2014; Dizon *et al.*, 2018).

Material Extrusion Additive Manufacturing is a technology where a thermoplastic polymer filament is pushed through a heated liquefier by a pinch roller mechanism. The molten polymer is extruded through a heated nozzle, and deposited onto a (heated) build platform or an already deposited layer, where it quickly solidifies (Turner *et al.*, 2014; Abbott *et al.*, 2018). By controlling the position of the heated nozzle and bed, complex 3D objects can be produced. The resulting end-product consists of stacked layers of partially bonded filaments with interstitial voids (Rodríguez *et al.*, 2001; Kousiatza and Karalekas, 2016).

Macroscopic mechanical properties of ME-AM products are mostly determined by *local* time-temperature profiles (initial fast cooling followed by fluctuation near or around the glass transition temperature (Kousiatza and Karalekas, 2016; Sun *et al.*,

2008; Seppala and Migler, 2016; Srinivas *et al.*, 2018)) and the resulting mesoscopic structure (void formation (Rodriguez *et al.*, 2000; Abbott *et al.*, 2018)) as a consequence of the processing step (Verbeeten *et al.*, 2015). By itself, these are influenced by the chosen printing parameters (Rodríguez *et al.*, 2001; Abbott *et al.*, 2018). As a function of (im)proper printing parameters, mechanical properties can be obtained that are lower than (Rodríguez *et al.*, 2001; Bellini and Güçeri, 2003; Tymrak *et al.*, 2014; Young *et al.*, 2018; Arbeiter *et al.*, 2018), similar to (Tymrak *et al.*, 2014; Lanzotti *et al.*, 2015; Verbeeten *et al.*, 2020) or even beyond (Chacón *et al.*, 2017; Song *et al.*, 2017; Arbeiter *et al.*, 2018; Verbeeten *et al.*, 2020) properties obtained by more conventional processing methods (*e.g.* injection molding or hot-press compression molding).

If the pure polymer properties are not sufficient for a specific application, mechanical properties are often improved by adding particles or (nano-)fibers. This method is more recently also applied for ME-AM, both with short-fiber reinforcements (Tekinalp *et al.*, 2014; Ning *et al.*, 2015; Quan *et al.*, 2016; Young *et al.*, 2018; Zhang *et al.*, 2018), nano-fibers/tubes (Shofner *et al.*, 2003; Zhang *et al.*, 2018), as well as continuous fibers (Dickson *et al.*, 2017; Naranjo-Lozada *et al.*, 2019). A review focused on fiber reinforced composites using ME-AM is given by Ferreira *et al.* (2019), while Van de Werken *et al.* (2020) wrote a review specified towards additively manufactured carbon fiber-reinforced composites. Both reviews, and supported by the authors' experience, mention several application fields, such as tools and fixtures or components with electrical and thermal conductivity (sensors, antennas), and industry sectors, *e.g.* aerospace, automotive, and energy, where AM composites are attractive in terms of cost, properties, and performance.

In the present paper, research is focused on Material Extrusion Additively Manufactured (ME-AM) Acrylonitrile-Butadiene-Styrene (ABS) components and its short carbon-fiber reinforced composites (CF-ABS). ABS is an important and widely used engineering thermoplastic for applications in the automotive, electronic and household appliances industries (Díez-Pascual and Gascón, 2013; Ceresana, 2016). It possesses good chemical resistance and surface appearance, excellent impact toughness, high dimensional stability, moderate mechanical properties, and easy processing characteristics at a relatively low cost (Martins *et al.*, 2010; Díez-Pascual and Gascón, 2013).

Several studies have investigated the mechanical properties of additively manufactured short CF-ABS components. The Oak Ridge National Laboratory group measured properties over a range of fiber loadings (10-40 wt%) and compared it to compression molded samples (Tekinalp *et al.*, 2014). Furthermore, they successfully applied short CF-ABS materials in a Big Area Additive Manufacturing (BAAM) system (Duty *et al.*, 2017). Ning *et al.* (2015) measured tensile and flexural properties for short CF-ABS samples with fiber loadings between 3 and 15 wt%. Quan *et al.* (2016) looked at 3D orthogonal, short CF-ABS preforms and measured the compressive behavior of these preforms. Young *et al.* (2018) developed a test method to determine interlayer, mode-I fracture toughness of additively manufactured CF-ABS specimen. Zhang *et al.* (2018) determined tensile and shear properties for ABS, CF-ABS and carbon nanotube reinforced ABS samples. They investigated different infill orientations, printing speed, and layer thickness. These last three papers employed the same CF-ABS material as used in the present study. Generally, they all observed improved tensile strength and elastic modulus by using carbon-fiber reinforced materials. Additionally, high fiber orientation and significant void formation and porosity was observed.

In order to use ME-AM components for structural applications, it is necessary to guarantee some minimal mechanical properties. Hence, it is most useful to be able to predict a ME-AM component's ultimate failure behavior. For that, the polymer's viscoelastic behavior has to be taken into account (Tervoort *et al.*, 1996; van Melick *et al.*, 2003; Klompen *et al.*, 2005a). Viscoelasticity in polymers is manifested in the initial stress-strain behavior up to yield (Tervoort *et al.*, 1996; van Breemen *et al.*, 2011) and the strain-rate dependence of the yield stress (Ree and Eyring, 1955; Haward and Thackray, 1968; Bauwens-Crowet *et al.*, 1969; Klompen and Govaert, 1999). Rodríguez *et al.* (2001) acknowledged that fact by measuring the strain-rate dependence of ABS material processed on a Stratasys machine. They showed that it could be well described by an Eyring rate equation. Vairis *et al.* (2016) also investigated the strain-rate sensitivity of two ABS materials using FDM technology. However, they applied a narrow strain-rate range of less then a decade and did not evaluate their results with an Eyring rate equation. As far as the authors know, strain-rate dependence for carbon-fiber reinforced ABS has not been measured so far.

The objective of this research paper is to quantify and analyze the strain-rate dependence of ME-AM tensile test samples fabricated with ABS and short CF-ABS materials. The infill orientation angle is varied to obtain test samples with longitudinal deposited strands and transverse deposited strands. In the remainder of this manuscript, an extruded and deposited filament is referred to as a strand. Thus, on the one hand, mechanical properties are obtained in the strand direction and, on the other hand, properties of bond formations between adjacent strands at a macroscopic scale are measured. Such measurements are paramount for the development of predictive ME-AM numerical tools to attain the inherent anisotropy of this technology. Moreover, the strain-rate dependence is not only important for measuring the viscoelastic behavior in short-term experiments. It is also important for long-term failure behavior, such as creep and fatigue, as was convincingly demonstrated in previous research (Janssen *et al.*, 2008; Kanters *et al.*, 2016). As an Eyring-type flow rule (Ree and Eyring, 1955) is able to accurately describe the viscoelastic strain-rate dependence (Bauwens-Crowet *et al.*, 1969), and it can be adequately incorporated in constitutive models for polymer materials (Boyce *et al.*, 1988; Wu and van der Giessen, 1993; Buckley and Jones, 1995; Klompen *et al.*, 2005b), its ability to predict the yield stress in uniaxial tensile tests is also evaluated.

2. Material and Methods

2.1. Material

Two different commercially available filaments were used for the present study: (i) a natural ABS filament; (ii) a CarbonX short carbon-fiber reinforced ABS filament (CF-ABS) having a 15% fiber volume fraction. Both filaments had a nominal diameter of $1.75\ mm$ and were obtained from 3DXTech (Grand Rapids, MI, USA). The specific gravity of the ABS filament is $1.05\ g/cm^3$ and of the CF-ABS filament is $1.11\ g/cm^3$, according to the filament producer. Recommended nozzle and bed temperature ranges are $220 - 240\ ^\circ C$ and $100 - 110\ ^\circ C$, respectively. All samples were fabricated from a single spool, and the filament was used as-received directly after opening the vacuum-sealed bag in which it was shipped.

2.2. *Material processing*

Tensile samples were manufactured on a German RepRap 350pro 3D printer (German RepRap GmbH, Feldkirchen, Germany) using a $0.4\ mm$ nozzle size. Sample dimensions are given in Figure 1(a). This tensile test specimen is based on specimen type 1BA according to the ISO 527-2 norm, but adapted to avoid fracture in the fillet (Verbeeten *et al.*, 2020).

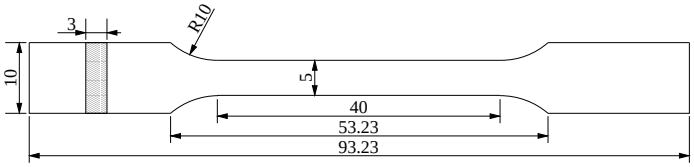

(a)

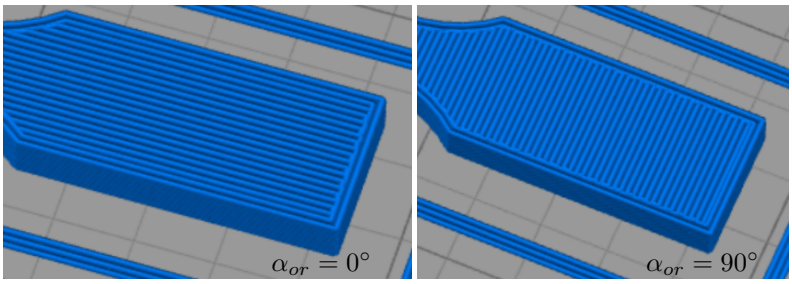

(b)

Figure 1: *(a)* Tensile test specimen dimensions in mm. *(b)* Close-ups of infill orientation angle.

An STL-file of the tensile sample was imported in the Simplify3D slicing software, copied 18 times and distributed in an equal manner over the surface representing the printer's XY plane. The printer parameters as given in Table 1 were used to generate two different G-code files that were handled by the German RepRap 350pro 3D printer to manufacture 18 equal tensile test samples: one G-code file for an infill orientation angle $\alpha_{or} = 0°$ (longitudinal), and one G-code file for $\alpha_{or} = 90°$ (transverse). Hence, a total of 4 sets were printed, 2 sets with ABS material and 2 sets with CF-ABS material. A close-up of the samples with the two different infill orientations is given in Figure 1(b).

Table 1: Processing parameters used to manufacture ME-AM tensile samples.

Processing parameter	Value
Nozzle diameter $[mm]$	0.40
Extrusion width $[mm]$	0.42
Layer height $[mm]$	0.20
Number of perimeters	2
Infill pattern	Rectilinear
Fill percentage	100%
Outline overlap	70%
Extrusion temperature $[^{\circ}C]$	245
Bed temperature T_b $[^{\circ}C]$	100
Printing speed v_p $[mm/s]$	25
Infill orientation angle α_{or}	0° or 90°

2.3. Mechanical characterization

An MTS Criterion C43.104 universal test system, equipped with a $10\ kN$ load cell, was applied to perform uniaxial tensile tests. All experiments were conducted at room temperature ($23\ ^{\circ}C$). For the tensile tests, constant linear strain rates were applied between $10^{-5}\ 1/s$ and $10^{-1}\ 1/s$. Three samples were used for each strain rate. The polymer's yield stresses were calculated from the first local stress maximum in the engineering stress-strain curves, which is a standard procedure. It is assumed that the material volume remains constant to apply the conversion from engineering to true yield stresses (Roetling, 1965; Bauwens-Crowet, 1973).

2.4. Apparent density

Since the resulting ME-AM products consist of stacked layers of partially bonded strands with interstitial voids (Rodríguez *et al.*, 2001; Kousiatza and Karalekas, 2016), logically, mechanical properties are affected by this voided mesostructure. In order

to determine the macroscopic material behavior of ME-AM processed samples, stress values were compensated for voids using the apparent density. Both mass and the external nominal volume for every single sample were measured to calculate its apparent density:

$$\rho_{app} = \frac{m_{sample}}{V_{sample}} \, . \tag{1}$$

Furthermore, an approximation of the porosity of the samples (in percentage) was determined by using the material reference density as given by the filament producer, *i.e.* $\rho_{ref} = 1.05 \; g/cm^3$ for ABS and $\rho_{ref} = 1.11 \; g/cm^3$ for CF-ABS:

$$\text{Porosity} = \frac{\rho_{ref} - \rho_{app}}{\rho_{ref}} \, . \tag{2}$$

2.5. SEM fractography

Following uniaxial tensile tests, the fracture surface of several samples were observed using a FEI Quanta 600 environmental scanning electron microscope (ESEM) (FEI Company Inc., Hillsboro, OR, USA). Additionally, an as-received filament portion prior to printing was also scanned. The samples were prepared by sputter-coating with an Au-coating. Samples were observed under vacuum and an accelerating voltage of $25.00 \; kV$.

2.6. Modeling

The deformation kinetics of polymers can be adequately described by a linear dependence of the yield stress on the logarithm of strain rate, on temperature, and on pressure (Roetling, 1965; Bauwens-Crowet *et al.*, 1969; Ward, 1971). Thus far, measurements on ABS materials have only shown thermorheologically simple behavior (Truss and Chadwick, 1976; Chen and Sauer, 1990; Bernal *et al.*, 1995; Louche *et al.*, 2009). An Eyring-type flow equation captures this behavior accurately:

$$\dot{\varepsilon}(\sigma, T, p) = \dot{\varepsilon}_0 \exp\left(-\frac{\Delta U}{RT}\right) \exp\left(-\frac{\mu p V^*}{kT}\right) \sinh\left(\frac{\sigma_y V^*}{kT}\right) \, . \tag{3}$$

Here, $\dot{\varepsilon}$ is the uniaxially applied strain rate, $\dot{\varepsilon}_0$ a rate constant, ΔU the activation energy, R the universal gas constant ($8.314472 \; J/(mol \; K)$), T the absolute temperature in K, μ is a dimensionless pressure dependence parameter, p the hydrostatic pressure, V^* the

activation volume, k is the Boltzmann's constant ($1.38054 \cdot 10^{-23}\ J/K$), and σ_y is the yield stress.

Since in this study only tensile tests at room temperature and atmospheric pressure are performed, the equation can be simplified. If written in terms of the yield stress as a function of strain rate, the equation becomes:

$$\sigma_y(\dot{\varepsilon}) = \frac{k\,T}{V^*} \sinh^{-1}\left[\frac{\dot{\varepsilon}}{\dot{\varepsilon}_0}\right] . \tag{4}$$

Note that true stress values are referred to in these previous two equations.

3. Results and Discussion

First, ME-AM ABS samples will be discussed and the differences between longitudinal and transverse samples due to anisotropy will be analyzed. Next, the CF-ABS samples will be looked at. Anisotropy for those samples will be treated and compared to the ABS sample sets. Finally, SEM fractography images of CF-ABS samples will be analyzed.

3.1. Material extrusion additively manufactured ABS samples

The mechanical stress-strain response of the longitudinal ($\alpha_{or} = 0°$) ABS samples is given in Figure 2. Every stress-strain curve in Figure 2(a) is the average of three test runs. This sample set has an average apparent density of $0.92\ g/cm^3$, compared to the material density of $1.05\ g/cm^3$ as given by the filament producer. That results in a rather high average porosity of 12.6% for this sample set.

Similar to any ABS material, the ME-AM samples started to show stress-whitening just before the yield stress, which intensified as strain increased. This whitening corresponds to the appearance of crazes (Truss and Chadwick, 1976). However, whitening was not uniform over the gauge section of the specimen samples. As a result, sample behavior was rather semi-ductile, and occasionally brittle, as can be observed in Figure 2(a). This in contrast to the results for injection molded ABS materials (Truss and Chadwick, 1976; Chen and Sauer, 1990) or the ABS monofilament results from Rodríguez *et al.* (2001) which showed ductile responses. However, the fused-deposition samples of Rodríguez *et al.* (2001) also demonstrated semi-ductile or brittle

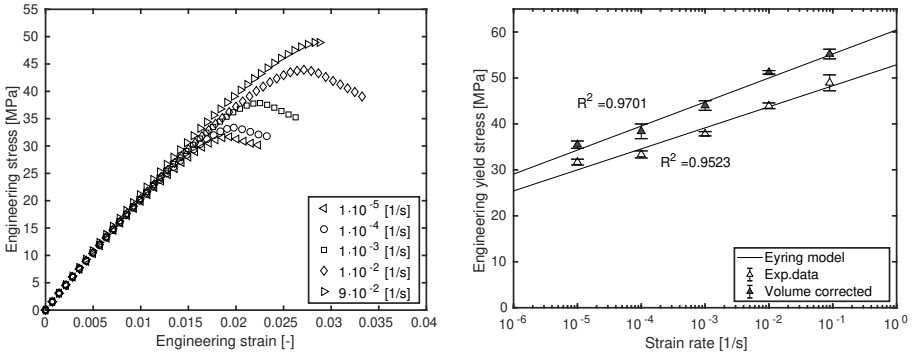

(a) (b)

Figure 2: Engineering stress/strain response of ABS samples, $\alpha_{or} = 0^{\circ}$. *(a)* Stress as a function of strain. *(b)* Yield stress and volume corrected yield stress as a function of logarithmic strain rate. Symbols are experimental results, solid lines are model predictions.

behavior. The voided structure is most likely to be responsible for that, as these voids reduce the nominal stress values and can generate strain-localization.

Since interstitial voids lower the stress values, that makes it more difficult to compare mechanical results between different sets in a macroscopic sense. Therefore, a compensation for the stress values of ME-AM samples is applied, by using the following equation:

$$\sigma_{y,vc}(\dot{\varepsilon}) = \sigma_y(\dot{\varepsilon}) \cdot \frac{\rho_{ref}}{\rho_{app}} \, . \tag{5}$$

Here, $\sigma_{y,vc}$ is the volume corrected yield stress, σ_y is the measured yield stress, ρ_{app} is the apparent density as calculated by Equation (1), and ρ_{ref} is the material density as given by the filament manufacturer. Thus, yield stresses are corrected for to represent "solid" samples, indicated as *volume corrected* results in Figure 2(b). This enables the comparison of effects of the printing process on macroscopic material behavior.

The longitudinal ME-AM sample set in this article shows stress values above (Rodríguez *et al.*, 2001; Bellini and Güçeri, 2003; Tymrak *et al.*, 2014) or similar to (Tymrak *et al.*, 2014) previously published results on ME-AM ABS samples, but below that of an injection-molded general-purpose grade ABS (Truss and Chadwick, 1976; Chen and Sauer, 1990). However, when compensated for the voided structure, yield stress values are similar to injection molded samples (Truss and Chadwick, 1976; Chen and Sauer, 1990).

As can be seen in Figure 2(b), the experimental strain-rate dependence of the yield stress data can be accurately described by Equation 4 with an activation volume and rate constant of $V^* = 1.72\ nm^3$ and $\dot{\varepsilon}_0 = 1.78 \cdot 10^{34}\ 1/s$, respectively. This gives a slope of 5.5 MPa/decade for the volume corrected true yield stresses, dropping down to 4.5 MPa/decade for the engineering yield stresses. These values are similar to the data published by Truss and Chadwick (1976) and Chen and Sauer (1990), and the ABS monofilament data of Rodríguez *et al.* (2001). The activation volume given here has a lower value, as it is based on the *volume corrected* true yield stress data, instead of the engineering yield stresses (Truss and Chadwick, 1976; Chen and Sauer, 1990; Rodríguez *et al.*, 2001).

The coefficient of determination R^2 is close to unity, and improves slightly for the volume corrected results. This indicates that an Eyring-type flow equation is able to correctly describe the thermorheologically simple behavior of this material as demonstrated by the strain-rate dependent yield stress data.

The elastic modulus E slightly increases from 2.1 GPa to 2.2 GPa with increasing strain rates $\dot{\varepsilon}$. Equally, the strain at yield ε_y rises from 1.9% to 2.8% in the measured strain-rate range. These are standard effects for viscoelastic materials.

The stress-strain response of the transverse ($\alpha_{or} = 90°$) ABS samples is shown in Figure 3. Again, the curves in Figure 3(a) are averages of three test runs. The apparent density for this sample set is equal to $0.94\ g/cm^3$, resulting in an average porosity of 10.1%. This is lower than for the longitudinal set. Since the time between the deposition of adjacent strands is shorter for the transverse direction, temperatures stay higher (Sun *et al.*, 2008; Abbott *et al.*, 2018), leading to more dense samples.

Similar to the longitudinal sample set, this transverse sample set also showed stress-whitening just before reaching the yield stress. Curiously, most samples showed more ductile behavior than the longitudinal samples, as can be seen when comparing Figure 2(a) to Figure 3(a). This demonstrates that adequate inter-strand bonds can be established with this printing parameter set. However, some of the samples showed brittle behavior, possibly resulting from a local defect. Thus, it indicates that the transverse sample set is more sensitive to these local defects than the longitudinal set. As expected, yield stresses for this transverse sample set are lower than for samples with

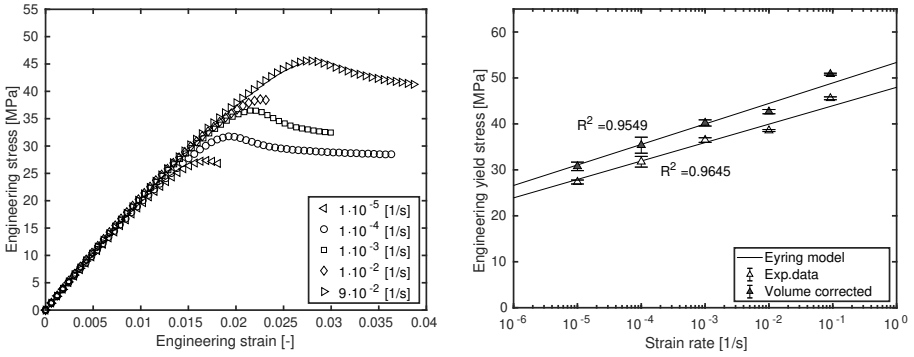

(a) (b)

Figure 3: Engineering stress/strain response of ABS samples, $\alpha_{or} = 90°$. *(a)* Stress as a function of strain. *(b)* Yield stress and volume corrected yield stress as a function of logarithmic strain rate. Symbols are experimental results, solid lines are model predictions.

$\alpha_{or} = 0°$.

In this set with an infill orientation of $\alpha_{or} = 90°$, the yield stress as a function of logarithmic strain rate can also be adequately captured with an Eyring-type flow equation (with a coefficient of determination R^2 again close to unity). The activation volume and rate constant were determined to be $V^* = 2.04\ nm^3$ and $\dot{\varepsilon}_0 = 5.90 \cdot 10^{33}\ 1/s$, respectively, giving a slope of 4.6 MPa/decade. This is a higher value for the activation volume, and a lower slope, compared to the longitudinal sample set. Rodríguez *et al.* (2001) also showed a difference in slope between the monofilament and printed sample results. They showed it to be related to the molecular orientation and stretch during the ME-AM process. It is assumed that this is responsible for the effects seen in our results. Thus, anisotropy is not only seen in the difference in yield stress at a single strain rate between various infill orientations, but also in its strain-rate dependence.

At increasing strain rates, strain at yield ε_y increases from 1.7% to 2.8%, while the elastic modulus E varies from 2.1 GPa to 2.2 GPa. Hence, the infill orientation does effect the yield stress values, the strain-rate dependence, and the ductility, but does not have a significant influence on the elastic modulus and the strain at yield in the measured strain-rate range.

3.2. Material extrusion additively manufactured CF-ABS samples

To establish the effect that short carbon-fibers have on ME-AM samples and to see to what extent mechanical properties can be improved, a CF-ABS filament is processed into samples with two distinct infill orientations. Printing parameters used for these samples are equal to the ones for producing the ME-AM ABS samples and are given in Table 1. Average stress-strain results for the CF-ABS samples with an infill orientation of $\alpha_{or} = 0°$ are shown in Figure 4. Stress-whitening could not be observed for these CF-ABS samples, as the samples' color is black. The apparent density of this CF-ABS set is $0.97\ g/cm^3$ (compared to a material density of $1.11\ g/cm^3$), leading to an approximate average porosity of 12.6%. Again a relatively high porosity value.

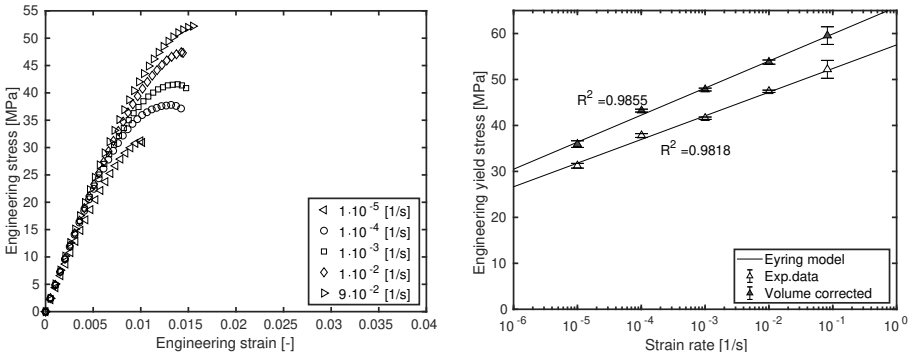

(a) (b)

Figure 4: Engineering stress/strain response of CF-ABS samples, $\alpha_{or} = 0°$. *(a)* Stress as a function of strain. *(b)* Yield stress and volume corrected yield stress as a function of logarithmic strain rate. Symbols are experimental results, solid lines are model predictions.

For the longitudinal CF-ABS samples, the elastic modulus E increases between 4.2 GPa and 4.9 GPa over the measured strain rate range. The yield stresses also augment, but to a significantly lesser degree. In fact, for the lowest strain rate, a similar yield stress is measured for the ABS and CF-ABS samples at $\alpha_{or} = 0°$. Thus, the effect of the carbon fibers is clearly noticeable for the elastic modulus. However, it has only a slight effect on the yield stress, which seems to be dominated by the ABS matrix material.

Due to the fact that the elastic modulus is enhanced, the strain at yield ε_y diminishes

to values between 1.0% and 1.6%. Additionally, the introduction of carbon fibers also makes the composite material behave in a brittle manner.

Again, the strain rate dependence of the yield stress can be excellently captured by equation 4, with a coefficient of determination R^2 even closer to unity than the previous two sets. An activation volume of $V^* = 1.56\ nm^3$ and a rate constant of $\dot{\varepsilon}_0 = 3.33 \cdot 10^{34}\ 1/s$ were determined to describe the experimental data. Hence, a slope of 6.0 MPa/decade is the result, which is higher than for the longitudinal ABS samples.

At the infill orientation $\alpha_{or} = 90°$, see Figure 5, CF-ABS samples show semi-ductile behavior. The yield stresses have significantly dropped compared to the $\alpha_{or} = 0°$ infill orientation. For these samples, the elastic modulus E varies from 2.7 GPa to 3.0 GPa, while strain at yield ε_y ranges from 1.6% to 2.0%.

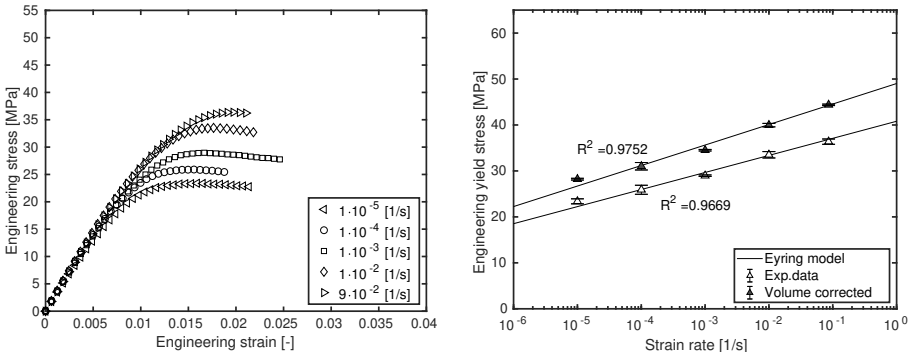

(a) (b)

Figure 5: Engineering stress/strain response of CF-ABS samples, $\alpha_{or} = 90°$. *(a)* Stress as a function of strain. *(b)* Yield stress and volume corrected yield stress as a function of logarithmic strain rate. Symbols are experimental results, solid lines are model predictions.

The apparent density for this sample set was measured to be $0.92\ g/cm^3$, which gives an average porosity of 16.8%, using the material density of $1.11\ g/cm^3$. This is, unexpectedly, an even higher value than for the $\alpha_{or} = 0°$ infill orientation. A plausible reason will be given in the SEM fractography subsection.

With an activation volume of $V^* = 2.04\ nm^3$ and a rate constant of $\dot{\varepsilon}_0 = 5.90 \cdot 10^{34}\ 1/s$, the experimental yield stresses over the measured strain rate rate can be ade-

quately described using an Eyring-type flow model. This is shown in Figure 5(b). Note that the activation volume is equal to the one for the unfilled ABS matrix, thus giving the same slope. This indicates that the deformation kinetics of this transverse CF-ABS sample set and the 90° unfilled ABS set are the same and, so, seem to be governed by the inter-strand bond strength of the ABS matrix material. The rate constant $\dot{\varepsilon}_0$ is a factor ten higher, as yield stresses are considerably lower.

Figure 6 compares results for the 4 sample sets. A substantially higher anisotropy is observed for the short carbon-fiber filled ABS material, compared to neat ABS material. There is a significant distinction in elastic modulus between infill orientations of $\alpha_{or} = 0^\circ$ and $\alpha_{or} = 90^\circ$ for this CF-ABS material, not detected for unfilled ABS, *i.e.* Figure 6(a). Furthermore, the yield stress difference between both infill orientations is substantially higher. Finally, the variation of the strain-rate dependence of the yield stresses, expressed in the activation volume of the Eyring-type flow equation, is also more pronounced, *i.e.* Figure 6(b).

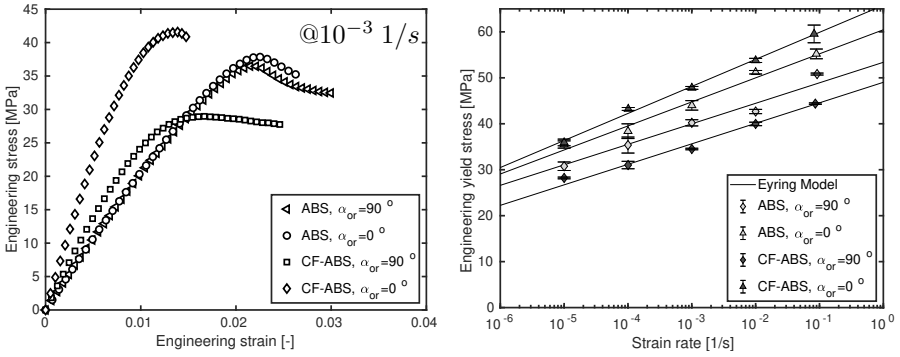

(a) (b)

Figure 6: Engineering stress/strain response of ABS and CF-ABS samples. *(a)* Experimental engineering stress as a function of strain $@10^{-3}\ 1/s$. *(b)* Volume corrected engineering yield stress as a function of logarithmic strain rate. Symbols are experimental results, solid lines are model predictions.

These differences find its origin in the addition of carbon-fibers, which provoke several effects. First, at the same processing temperature, the viscosity of the CF-ABS material is higher (Quan *et al.*, 2016), which has a major effect on the bonding between adjacent strands (Turner *et al.*, 2014). Second, after strand deposition, the

temperature of the material drops more rapidly (Young *et al.*, 2018) as a consequence of an increased thermal conductivity (Tekinalp *et al.*, 2014). Third, the addition of fibers provokes the appearance of internal voids inside the strands (Tekinalp *et al.*, 2014; Quan *et al.*, 2016; Zhang *et al.*, 2018). Last, the short carbon-fibers are highly aligned in the printing direction (Tekinalp *et al.*, 2014; Quan *et al.*, 2016; Young *et al.*, 2018; Zhang *et al.*, 2018). These last two effects will be shown with SEM fractography images in the next subsection.

A higher viscosity at the same temperature, faster cooling, and the presence of fibers, all provoke that the polymer molecules are hindered in flow. Furthermore, high fiber alignment will induce higher polymer molecule orientation and stretch (Tekinalp *et al.*, 2014). As a result, the sintering process between adjacent strands, which is governed by a diffusion bond mechanism (Turner *et al.*, 2014; Kousiatza and Karalekas, 2016; Seppala and Migler, 2016), is slower and the bond strength is severely reduced. These effects are manifested in the results shown in this manuscript. On the one hand, the CF-ABS sample set with an infill orientation of $\alpha_{or} = 0^\circ$ shows higher yield stresses and a lower activation volume due to the fiber and molecular orientations. On the other hand, the transverse CF-ABS sample set shows lower yield stresses due to poorer inter-strand bonds, which also results in a semi-ductile fracture behavior, compared to the more ductile behavior of some of the ABS samples at $\alpha_{or} = 90^\circ$. Besides, the inner-strand voids affect this transverse sample set more, as the ultimate mechanical properties (*i.e.* the yield stresses) are mostly determined by the ABS matrix material and significantly less by the carbon fibers, which are predominantly aligned transverse to the loading direction. The fact that the 90° CF-ABS samples show a higher elastic modulus E than the ABS samples is by reason of the 2 perimeters which are used to produce the samples. In those perimeters, as will be shown in the next subsection, fibers are aligned in the tensile direction.

By analyzing Figure 6(b) and comparing the values of the activation volumes for these four sets, molecular orientation seems to affect the results (Rodríguez *et al.*, 2001). The two activation volumes of the two sample sets with infill orientation $\alpha_{or} = 90^\circ$ are equal. In these sets, the main printing direction is perpendicular to the loading direction. Accordingly, both fiber as well as molecular orientation will also be

predominantly in this transverse direction. As a consequence, fiber and molecular orientation do not affect the deformation kinetics and activation volumes are equal, giving the highest values of all four sets. On the contrary, as printing and loading direction in the ABS sample set with $\alpha_{or} = 0^{\circ}$ are the same, molecular orientation will affect the deformation kinetics and the activation volume value lowers (Rodríguez *et al.*, 2001), manifested by a higher slope. Finally, the 0° CF-ABS sample set has carbon fibers aligned in the printing and loading direction. This will induce additional polymer molecule orientation and stretch (Tekinalp *et al.*, 2014). Consequently, this set displays the lowest activation volume and the highest slope. These findings are in accordance with research on yielding of oriented polypropylene, polyethylene, and polyoxymethylene (van Erp *et al.*, 2013; Senden *et al.*, 2013; Coates and Ward, 1978).

Note that in the current study, the focus is not on the optimization of ME-AM process parameters to obtain the best possible mechanical properties. Rather, the effect of the addition of short carbon-fiber reinforcement on the mechanical properties is investigated and, therefore, the same printing parameters are applied for both materials. It is clear from the transverse CF-ABS results, that properties can most likely be improved by adjusting the process temperature parameters in order to obtain better inter-strand bonds.

3.3. SEM fractography

A cross-section of the as-received CF-ABS filament was analyzed by SEM micrography. As can be seen in Figure 7, the short carbon-fibers are well distributed throughout the filament feedstock material and are strongly aligned in the filament long direction. Fiber diameter was determined to be $\sim 8\ \mu m$, equal to what was measured by Quan *et al.* (2016). The SEM micrographs also show the low interaction between fibers and matrix material. Significant fiber pull-out can be observed, with fibers that are completely separated from the ABS matrix indicating poor wetting, which confirms the previously stated observation. This was also mentioned by Quan *et al.* (2016), Young *et al.* (2018), and Zhang *et al.* (2018) who used the same CF-ABS material as employed in this study. In the central zone of the filament cross-section, large voids can be observed, similar to what was seen by Quan *et al.* (2016) and Zhang *et al.*

(2018). The presence of carbon-fibers provokes inner-strand porosity (Tekinalp *et al.*, 2014; Ning *et al.*, 2015; Quan *et al.*, 2016; Dickson *et al.*, 2017; Zhang *et al.*, 2018), which seems to be the reason for the low apparent density in CF-ABS materials.

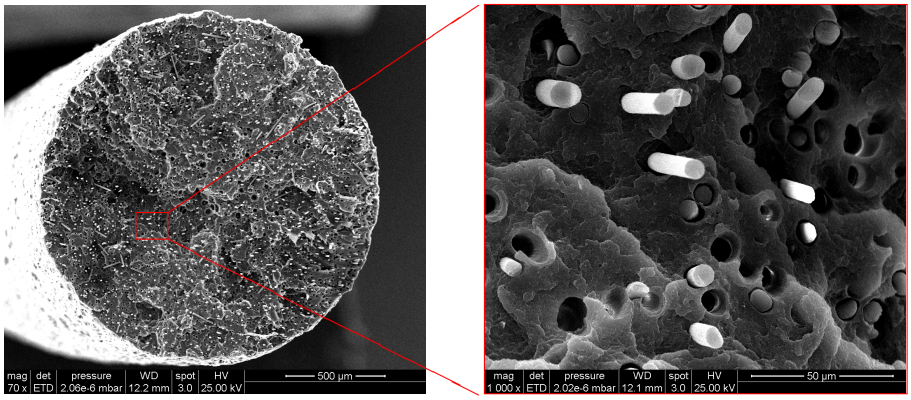

(a) (b)

Figure 7: SEM micrographs of the as-received CF-ABS filament cross-section.

Figure 8 shows representative SEM micrographs of the fracture surface of an ME-AM CF-ABS sample with $\alpha_{or} = 0°$. Inter-layer, inter-strand, and inner-strand voids can be detected for this sample. Especially in the two perimeter strands, the inter-layer voids are more pronounced. Furthermore, inter-strand porosity are more marked in the two top layers (not shown here). Both these effects are due to the temperature profile the sample has undergone during processing, which are marked by lower average temperatures on these top layers.

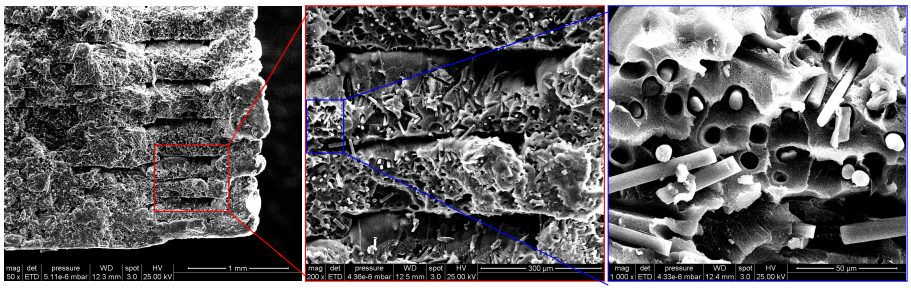

(a) (b) (c)

Figure 8: SEM micrographs of the ME-AM CF-ABS sample fracture cross-section, $\alpha_{or} = 0°$.

What can also be seen in Figure 8, is that the carbon fibers are preferentially oriented in the printing direction, which is perpendicular to the cross-section shown. Again, poor fiber-matrix interfacial adhesion is detected, as manifested by the prominent holes left behind by the fiber pull-out and the visible fiber ends sticking out of the matrix material. Notice also some loose fiber parts that seem to be lying on top of the surface. As was also detected by Young *et al.* (2018), there are hardly any carbon fibers that bridge between adjacent strands or layers. However, diffusion of the matrix material across strands and layers can be observed. Furthermore, plastic deformation of the ABS matrix is also noticed, indicating that, despite the macroscopic behavior being brittle, the matrix material does deform in a ductile manner. Although not shown here, no significant differences were observed for samples that were characterized at different strain rates.

In Figure 9, representative SEM images are viewed corresponding to the fracture surface of a transversely loaded ME-AM CF-ABS sample. Images are taken from the zone where both the two perimeter strands and the 90° infill is visible. On the left part of image 9(a), oblong cross-sections of the perimeter strands can be identified, surrounded by triangle-shaped and, occasionally, diamond-shaped voids. On the right side of that same image, the infill strands can be recognized by the horizontally oriented carbon fibers.

From Figures 9(a) and 9(c), one can see that fiber orientation is mainly perpendicular to the fracture surface in the two perimeter strands. This orientation is responsible for the value of the elastic modulus for this sample set. Additionally, large and more numerous inner-strand voids can be observed, compared to Figure 8. This is the probable cause for the lower apparent density for these samples with infill orientation $\alpha_{or} = 90^\circ$. Plastic deformation of the ABS matrix material can again be spotted in these images.

Preferential orientation of the carbon fibers in the printing direction can also be perceived for the infill strands (Figures 9(a), 9(b), and 9(d)). Holes where fibers have been located are left behind on the fracture surface, confirming low fiber-matrix adhesion. On this fracture surface, ductile ABS matrix plastic deformation is again seen. This confirms what was seen in the mechanical property results, namely that it is the poly-

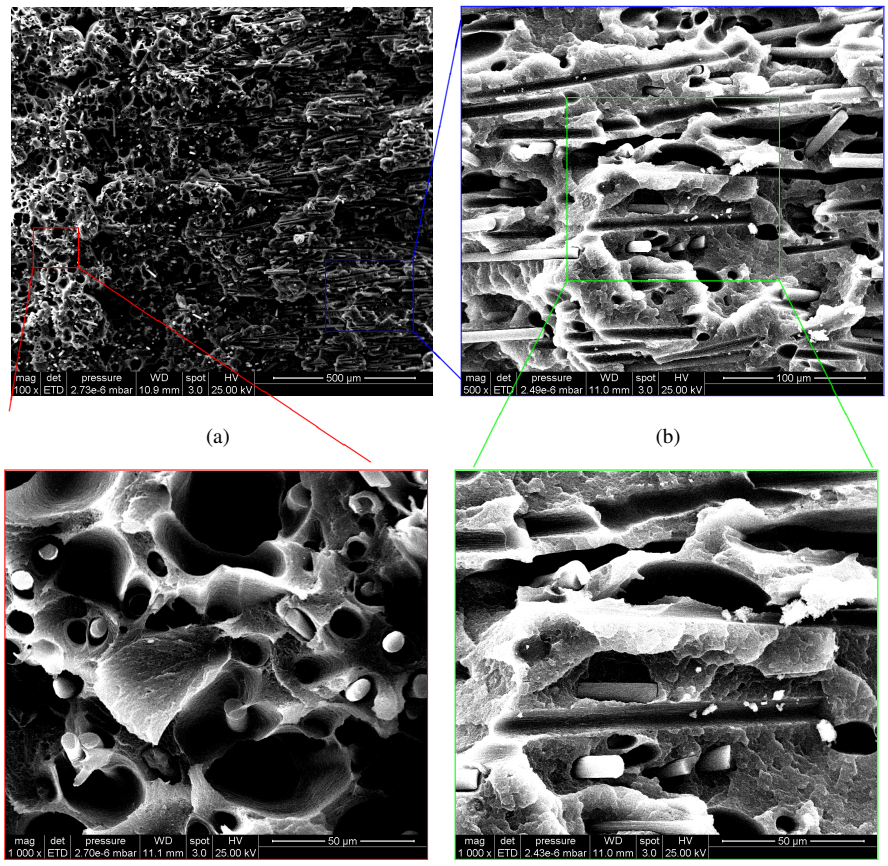

(a) (b)

(c) (d)

Figure 9: SEM micrographs of the ME-AM CF-ABS sample fracture cross-section, $\alpha_{or} = 90°$.

mer matrix that mainly determines the properties at an infill orientation of $\alpha_{or} = 90°$, and that the fibers hardly support any force due to the low fiber-matrix adhesion.

4. Conclusions

The strain-rate dependence of the yield stress for unfilled ABS and short carbon-fiber reinforced ABS materials was determined for tensile test samples produced via material extrusion additive manufacturing (ME-AM). For all samples, the apparent density was measured and used to apply a compensation of stresses in order to account for the voided structure, which is inherent to ME-AM techniques. This enables

a comparison between "solid" samples and establish the printing process effects on macroscopic material behavior. One of the printing parameters was varied, *i.e.* the infill orientation angle, in order to investigate its influence on the macroscopic tensile properties and strain-rate dependence, both for the unfilled as well as the reinforced material.

Two extreme infill orientation angles were measured: (i) in the strand direction ($\alpha_{or} = 0°$) and (ii) between adjacent strands ($\alpha_{or} = 90°$). These two angles are useful for refining predictive numerical tools. However, to detect the orientation dependence of the yield stress, it will be necessary to measure a range of infill angles (Senden *et al.*, 2013). Yet, that was outside the scope of the current study and will be addressed in future research.

In general, and as also observed in the results of the present study, ME-AM components demonstrate lower stress values compared to parts fabricated by more conventional processing methods, *e.g.* injection or compression molding. However, if compensated for by the apparent density, the present measured ABS yield stress values are close to previously published results of injection molded samples (Truss and Chadwick, 1976; Chen and Sauer, 1990).

Anisotropy due to infill orientation is observed for both ABS as well as short carbon-fiber reinforced ABS (CF-ABS) materials. Yet, for the printing parameter set used here, a more enhanced anisotropy is observed for the CF-ABS samples. As for the neat ABS material, yield stresses and strain-rate dependence is higher for the samples with infill angle $0°$ compared to samples with $90°$ infill angle. Additionally, for the CF-ABS material, the yield stress difference is significantly greater, the strain-rate dependence between both infill orientations is more pronounced, and the elastic modulus is distinct for the longitudinal ($\alpha_{or} = 0°$) and transverse ($\alpha_{or} = 90°$) samples.

Results for all sample sets demonstrated thermorheologically simple material behavior. This strain-rate dependent behavior can be well described with an Eyring-type flow rule. The ABS and CF-ABS sample set with an infill orientation angle $\alpha_{or} = 90°$ displayed an equal strain-rate dependence, manifested by the same value for the activation volume. This hints towards the failure deformation kinetics to be governed by the ABS matrix material for these two sample sets.

Based on observations of previous research (Rodríguez *et al.*, 2001; van Erp *et al.*, 2013; Senden *et al.*, 2013; Coates and Ward, 1978), molecular orientation seems to be the reason for the enhanced slopes of the strain-rate dependence for the longitudinal ($\alpha_{or} = 0^\circ$) sample sets. For ABS samples with $\alpha_{or} = 0^\circ$, the printing direction, and as a consequence also molecular orientation (Rodríguez *et al.*, 2001), is aligned in the loading direction, affecting the deformation kinetics and strain-rate dependence. For the longitudinal CF-ABS samples, the carbon fibers are preferentially oriented in the printing direction, inducing an additional polymer molecule orientation (Tekinalp *et al.*, 2014). At the same time, these CF-ABS samples show the highest strain-rate dependence.

The presence of carbon-fibers provokes inner-strand porosity (Tekinalp *et al.*, 2014; Ning *et al.*, 2015; Quan *et al.*, 2016; Dickson *et al.*, 2017; Zhang *et al.*, 2018), affecting negatively the mechanical properties. These inner-strand voids were clearly visible in the SEM fractography images. Similarly, it was shown that fiber-matrix adhesion was poor. Improvement of this adhesion is an opportunity to increase the CF-ABS composite properties. As an additional effect, such an improvement may well lead to a reduction of the inner-strand voids. Ultimately, since the addition of carbon-fiber reinforcement changes the viscosity and thermal conductivity of the material, it is suggested to adjust the ME-AM process parameters in order to obtain better inter-strand bonds. That will result in superior mechanical properties as well.

The experimental results shown in the present paper indicate that strain-rate dependence of the yield stress is anisotropic and can be satisfactorily predicted by an Eyring-type flow rule. This is an important *initial* finding that can help to further develop predictive numerical tools for ME-AM. Previously, it was shown that these kind of flow rules can be adequately incorporated in constitutive models for polymer materials (Boyce *et al.*, 1988; Wu and van der Giessen, 1993; Buckley and Jones, 1995; Klompen *et al.*, 2005b). Furthermore, strain-rate dependence is not only important to determine short-term viscoelastic material behavior, but also has its effect on long-term failure behavior, such as creep (Kanters *et al.*, 2016) and fatigue (Janssen *et al.*, 2008). Finally, in order to more accurately corroborate anisotropic yielding in ME-AM components, it is recommended to measure strain-rate dependence for a more complete

range of infill orientations, as was shown for anisotropy detected in injection molding (Senden *et al.*, 2013).

Acknowledgements: The authors gratefully thank Pedro Luis Sánchez Ortega and José María Cámara Nebreda of the DINper research group at the Universidad de Burgos for making use of their laboratory facilities and initial help with ME-AM processing.

This research did not receive any specific grant from funding agencies in the public, commercial, or not-for-profit sectors.

References

Abbott, A., Tandon, G., Bradford, R., Koerner, H., and Baur, J. (2018). "Process-structure-property effects on ABS bond strength in fused filament fabrication". *Addit. Manuf.*, Vol. 19, pp. 29–38. doi:http://dx.doi.org/10.1016/j.addma.2017.11.002.

Arbeiter, F., Spoerk, M., Wiener, J., Gosch, A., and Pinter, G. (2018). "Fracture mechanical characterization and lifetime estimation of near-homogeneous components produced by fused filament fabrication". *Polym. Test.*, Vol. 66, pp. 105–113. doi: https://dx.doi.org/10.1016/j.polymertesting.2018.01.002.

Bauwens-Crowet, C. (1973). "The compression yield behaviour of polymethyl methacrylate over a wide range of temperatures and strain-rates". *J. Mater. Sci.*, Vol. 8 No. 7, pp. 968–979. doi:https://dx.doi.org/10.1007/BF00756628.

Bauwens-Crowet, C., Bauwens, J., and Homès, G. (1969). "Tensile yieldstress behavior of glassy polymers". *J. Polym. Sci. Part A-2: Polym. Phys.*, Vol. 7 No. 4, pp. 735–742. doi:http://dx.doi.org/10.1002/pol.1969.160070411.

Bellini, A. and Güçeri, S. (2003). "Mechanical characterization of parts fabricated using fused deposition modeling". *Rapid Prototyp. J.*, Vol. 9 No. 4, pp. 252–264. doi:http://dx.doi.org/10.1108/13552540310489631.

Bernal, C., Frontini, P., Sforza, M., and Bibbó, M. (1995). "Microstructure, deformation, and fracture behavior of commercial ABS resins". *J. Appl. Polym. Sci.*, Vol. 58 No. 1, pp. 1–10. doi:https://dx.doi.org/10.1002/app.1995.070580101.

Boyce, M., Parks, D., and Argon, A. (1988). "Large inelastic deformation of glassy polymers. part I: rate dependent constitutive model". *Mech. Mater.*, Vol. 7 No. 1, pp. 15–33. doi:http://dx.doi.org/10.1016/0167-6636(88)90003-8.

van Breemen, L., Klompen, E., Govaert, L., and Meijer, H. (2011). "Extending the EGP constitutive model for polymer glasses to multiple relaxation times". *J. Mech. Phys. Solids*, Vol. 59 No. 10, pp. 2191–2207. doi:http://dx.doi.org/10.1016/j.jmps.2011.05.001.

Buckley, C. and Jones, D. (1995). "Glass-rubber constitutive model for amorphous polymers near the glass transition". *Polymer*, Vol. 36 No. 17, pp. 3301–3312. doi:http://dx.doi.org/10.1016/0032-3861(95)99429-X.

Ceresana (2016). *Market Study: Engineering Plastics*. Ceresana, Constance, 2nd edition.

Chacón, J., Caminero, M., García-Plaza, E., and Núñez, P. (2017). "Additive manufacturing of PLA structures using fused deposition modelling: Effect of process parameters on mechanical properties and their optimal selection". *Mater. Des.*, Vol. 124, pp. 143–157. doi:http://dx.doi.org/10.1016/j.matdes.2017.03.065.

Chen, C. and Sauer, J. (1990). "Yield and fracture mechanisms in ABS". *J. Appl. Polym. Sci.*, Vol. 40 No. 3-4, pp. 503–521. doi:http://dx.doi.org/10.1002/app.1990.070400317.

Coates, P. and Ward, I. (1978). "The plastic deformation behaviour of linear polyethylene and polyoxymethylene". *J. Mater. Sci.*, Vol. 13 No. 9, pp. 1957–1970. doi:http://dx.doi.org/10.1007/BF00552903.

Dickson, A., Barry, J., McDonnell, K., and Dowling, D. (2017). "Fabrication of continuous carbon, glass and Kevlar fibre reinforced polymer composites using additive manufacturing". *Addit. Manuf.*, Vol. 16, pp. 146–152. doi:http://dx.doi.org/10.1016/j.addma.2017.06.004.

Díez-Pascual, A. and Gascón, D. (2013). "Carbon Nanotube Buckypaper Reinforced AcrylonitrileButadieneStyrene Composites for Electronic Applications". *ACS Appl.*

Mater. Interfaces, Vol. 5 No. 22, pp. 12107–12119. doi:https://dx.doi.org/10.1021/am4039739.

Dizon, J., Espera Jr., A., Chen, Q., and Advincula, R. (2018). "Mechanical characterization of 3D-printed polymers". *Addit. Manuf.*, Vol. 20, pp. 44–67. doi:http://dx.doi.org/10.1016/j.addma.2017.12.002.

Duty, C., Kunc, V., Compton, B., Post, B., Erdman, D., Smith, R., Lind, R., Lloyd, P., and Love, L. (2017). "Structure and mechanical behavior of Big Area Additive Manufacturing (BAAM) materials". *Rapid Prototyp. J.*, Vol. 23 No. 1, pp. 181–189. doi:http://dx.doi.org/10.1108/RPJ-12-2015-0183.

van Erp, T., Govaert, L., and Peters, G. (2013). "Mechanical Performance of Injection-Molded Poly(propylene): Characterization and Modeling". *Macromol. Mater. Eng.*, Vol. 298 No. 3, pp. 348–358. doi:http://dx.doi.org/10.1002/mame.201200116.

Ferreira, I., Machado, M., Alves, F., and Torres Marques, A. (2019). "A review on fibre reinforced composite printing via FFF". *Rapid Prototyp. J.*, Vol. 25 No. 6, pp. 972–988. doi:http://dx.doi.org/10.1108/RPJ-01-2019-0004.

Haward, R. and Thackray, G. (1968). "The Use of a Mathematical Model to Describe Isothermal Stress-Strain Curves in Glassy Thermoplastics". *Proc. Royal Soc. London, Series A: Math., Phys. Eng. Sci.*, Vol. 302 No. 1471, pp. 453–472. doi:http://dx.doi.org/10.1098/rspa.1968.0029.

ISO/ASTM 52900 (2015). "Additive manfucturing - General principles - Terminology".

Janssen, R., de Kanter, D., Govaert, L., and Meijer, H. (2008). "Fatigue Life Predictions for Glassy Polymers: A Constitutive Approach". *Macromolecules*, Vol. 41 No. 7, pp. 2520–2530. doi:http://dx.doi.org/10.1021/ma071273i.

Kanters, M., Remerie, K., and Govaert, L. (2016). "A New Protocol for Accelerated Screening of Long-Term Plasticity-Controlled Failure of Polyethylene Pipe Grades". *Polym. Eng. Sci.*, Vol. 56 No. 6, pp. 676–688. doi:https://dx.doi.org/10.1002/pen.24294.

Klompen, E., Engels, T., van Breemen, L., Schreurs, P., Govaert, L., and Meijer, H. (2005a). "Quantitative Prediction of Long-Term Failure of Polycarbonate". *Macromolecules*, Vol. 38 No. 16, pp. 7009–7017. doi:http://dx.doi.org/10.1021/ma0504973.

Klompen, E., Engels, T., Govaert, L., and Meijer, H. (2005b). "Modeling of the Postyield Response of Glassy Polymers: Influence of Thermomechanical History". *Macromolecules*, Vol. 38 No. 16, pp. 6997–7008. doi:http://dx.doi.org/10.1021/ma050498v.

Klompen, E. and Govaert, L. (1999). "Nonlinear Viscoelastic Behaviour of Thermorheologically Complex Materials". *Mech. Time-Dep. Mater.*, Vol. 3 No. 1, pp. 49–69. doi:http://dx.doi.org/10.1023/A:1009853024441.

Kousiatza, C. and Karalekas, D. (2016). "In-situ monitoring of strain and temperature distributions during fused deposition modeling process". *Mater. Des.*, Vol. 97, pp. 400–406. doi:https://dx.doi.org/10.1016/j.matdes.2016.02.099.

Lanzotti, A., Grasso, M., Staiano, G., and Martorelli, M. (2015). "The impact of process parameters on mechanical properties of parts fabricated in PLA with an open-source 3-D printer". *Rapid Prototyp. J.*, Vol. 21 No. 5, pp. 604–617. doi:http://dx.doi.org/10.1108/RPJ-09-2014-0135.

Louche, H., Piette-Coudol, F., Arrieux, R., and Issartel, J. (2009). "An experimental and modeling study of the thermomechanical behavior of an ABS polymer structural component during an impact test". *Int. J. Impact Eng.*, Vol. 36 No. 6, pp. 847–861. doi:https://dx.doi.org/10.1016/j.ijimpeng.2008.09.007.

Martins, J., Klohn, T., Bianchi, O., Fiorio, R., and Freire, E. (2010). "Dynamic mechanical, thermal, and morphological study of ABS/textile fiber composites". *Polym. Bull.*, Vol. 64 No. 5, pp. 497–510. doi:https://dx.doi.org/10.1007/s00289-009-0200-6.

van Melick, H., Govaert, L., and Meijer, H. (2003). "Localisation phenomena in glassy

polymers: influence of thermal and mechanical history". *Polymer*, Vol. 44 No. 12, pp. 3579–3592. doi:http://dx.doi.org/10.1016/S0032-3861(03)00089-2.

Naranjo-Lozada, J., Ahuett-Garza, H., Orta-Castañón, P., Verbeeten, W., and Sáiz-González, D. (2019). "Tensile properties and failure behavior of chopped and continuous carbon fiber composites produced by Additive Manufacturing". *Addit. Manuf.*, Vol. 26, pp. 227–241. doi:https://dx.doi.org/10.1016/j.addma.2018.12.020.

Ning, F., Cong, W., Qiu, J., Wei, J., and Wang, S. (2015). "Additive manufacturing of carbon fiber reinforced thermoplastic composites using fused deposition modeling". *Compos. Part B*, Vol. 80, pp. 369–378. doi:http://dx.doi.org/10.1016/j.compositesb.2015.06.013.

Quan, Z., Larimore, Z., Wu, A., Yu, J., Qin, X., Mirotznik, M., Suhr, J., Byun, J.H., Oh, Y., and Chou, T.W. (2016). "Microstructural design and additive manufacturing and characterization of 3D orthogonal short carbon fiber/acrylonitrile-butadiene-styrene preform and composite". *Compos. Sci. Technol.*, Vol. 126, pp. 139–148. doi:http://dx.doi.org/10.1016/j.compscitech.2016.02.021.

Ree, T. and Eyring, H. (1955). "Theory of Non-Newtonian Flow. I. Solid Plastic System". *J. Appl. Phys.*, Vol. 26 No. 7, pp. 793–800. doi:http://dx.doi.org/10.1063/1.1722098.

Rodriguez, J., Thomas, J., and Renaud, J. (2000). "Characterization of the mesostructure of fused-deposition acrylonitrile-butadiene-styrene materials". *Rapid Prototyp. J.*, Vol. 6 No. 3, pp. 175–185. doi:http://dx.doi.org/10.1108/13552540010337056.

Rodríguez, J., Thomas, J., and Renaud, J. (2001). "Mechanical behavior of acrylonitrile butadiene styrene (ABS) fused deposition materials. Experimental investigation". *Rapid Prototyp. J.*, Vol. 7 No. 3, pp. 148–158. doi:http://dx.doi.org/10.1108/13552540110395547.

Roetling, J. (1965). "Yield Stress Behaviour of Polymethylmethacrylate". *Polymer*, Vol. 6 No. 6, pp. 311–317. doi:http://dx.doi.org/10.1016/0032-3861(65)90081-9.

Senden, D., Peters, G., Govaert, L., and van Dommelen, J. (2013). "Anisotropic yielding of injection molded polyethylene: Experiments and modeling". *Polymer*, Vol. 54 No. 21, pp. 5899–5908. doi:http://dx.doi.org/10.1016/j.polymer.2013.08.047.

Seppala, J. and Migler, K. (2016). "Infrared thermography of welding zones produced by polymer extrusion additive manufacturing". *Addit. Manuf.*, Vol. 12, pp. 71–76. doi:https://dx.doi.org/10.1016/j.addma.2016.06.007.

Shofner, M., Lozano, K., Rodríguez-Maciías, F., and Barrera, E. (2003). "Nanofiber-Reinforced Polymers Prepared by Fused Deposition Modeling". *J. Appl. Polym. Sci.*, Vol. 89 No. 11, pp. 3081–3090. doi:https://dx.doi.org/10.1002/app.12496.

Song, Y., Li, Y., Song, W., Yee, K., Lee, K.Y., and Tagarielli, V. (2017). "Measurements of the mechanical response of unidirectional 3D-printed PLA". *Mater. Des.*, Vol. 123, pp. 154–164. doi:https://dx.doi.org/10.1016/j.matdes.2017.03.051.

Srinivas, V., van Hooy-Corstjens, C., and Harings, J. (2018). "Correlating molecular and crystallization dynamics to macroscopic fusion and thermodynamic stability in fused deposition modeling; a model study on polylactides". *Polymer*, Vol. 142, pp. 348–355. doi:http://dx.doi.org/10.1016/j.polymer.2018.03.063.

Sun, Q., Rizvi, G., Bellehumeur, C., and Gu, P. (2008). "Effect of processing conditions on the bonding quality of FDM polymer filaments". *Rapid Prototyp. J.*, Vol. 14 No. 2, pp. 72–80. doi:http://dx.doi.org/10.1108/13552540810862028.

Tekinalp, H., Kunc, V., Velez-Garcia, G., Duty, C., Love, L., Naskar, A., Blue, C., and Ozcan, S. (2014). "Highly oriented carbon fiberpolymer composites via additive manufacturing". *Compos. Sci. Technol.*, Vol. 105, pp. 144–150. doi:http://dx.doi.org/10.1016/j.compscitech.2014.10.009.

Tervoort, T., Klompen, E., and Govaert, L. (1996). "A multi-mode approach to finite, three-dimensional, nonlinear viscoelastic behavior of polymer glasses". *J. Rheol.*, Vol. 40 No. 5, pp. 779–797. doi:http://dx.doi.org/10.1122/1.550755.

Truss, R. and Chadwick, G. (1976). "Tensile deformation behaviour of ABS polymers". *J. Mater. Sci.*, Vol. 11 No. 1, pp. 111–117. doi:http://dx.doi.org/10.1007/BF00541081.

Turner, B., Strong, R., and Gold, S. (2014). "A review of melt extrusion additive manufacturing processes: I. Process design and modeling". *Rapid Prototyp. J.*, Vol. 20 No. 3, pp. 192–204. doi:http://dx.doi.org/10.1108/RPJ-01-2013-0012.

Tymrak, B., Kreiger, M., and Pearce, J. (2014). "Mechanical properties of components fabricated with open-source 3-D printers under realistic environmental conditions". *Mater. Des.*, Vol. 58, pp. 242–246. doi:http://dx.doi.org/10.1016/j.matdes.2014.02.038.

Vairis, A., Petousis, M., Vidakis, N., and Savvakis, K. (2016). "On the Strain Rate Sensitivity of Abs and Abs Plus Fused Deposition Modeling Parts". *J. Mater. Eng. Perf.*, Vol. 25 No. 9, pp. 3558–3565. doi:http://dx.doi.org/10.1007/s11665-016-2198-x.

Verbeeten, W., Kanters, M., Engels, T., and Govaert, L. (2015). "Yield stress distribution in injection-moulded glassy polymers". *Polym. Int.*, Vol. 64 No. 11, pp. 1527–1536. doi:http://dx.doi.org/10.1002/pi.4898.

Verbeeten, W., Lorenzo-Bañuelos, M., and Arribas-Subiñas, P. (2020). "Anisotropic rate-dependent mechanical behavior of Poly(Lactic Acid) processed by Material Extrusion Additive Manufacturing". *Addit. Manuf.*, Vol. 31, p. 100968. doi:http://dx.doi.org/10.1016/j.addma.2019.100968.

Ward, I. (1971). "Review: The Yield Behaviour of Polymers". *J. Mater. Sci.*, Vol. 6 No. 11, pp. 1397–1417. doi:http://dx.doi.org/10.1007/BF00549685.

Van de Werken, N., Tekinalp, H., Khanbolouki, P., Ozcan, S., Williams, A., and Tehrani, M. (2020). "Additively manufactured carbon fiber-reinforced composites: State of the art and perspective". *Addit. Manuf.*, Vol. 31, p. 100962. doi:http://dx.doi.org/10.1016/j.addma.2019.100962.

Wu, P. and van der Giessen, E. (1993). "On improved network models for rubber elasticity and their applications to orientation hardening in glassy polymers". *J.*

Mech. Phys. Solids, Vol. 41 No. 3, pp. 427–456. doi:http://dx.doi.org/10.1016/0022-5096(93)90043-F.

Young, D., Wetmore, N., and Czabaj, M. (2018). "Interlayer fracture toughness of additively manufactured unreinforced and carbon-fiber-reinforced acrylonitirle butadiene styrene". *Addit. Manuf.*, Vol. 22, pp. 508–515. doi:http://dx.doi.org/10.1016/j.addma.2018.02.023.

Zhang, W., Cotton, C., J., S., Heider, D., Gu, B., Sun, B., and Chou, T.W. (2018). "Interfacial bonding strength of short carbon fiber/acrylonitrile-butadiene-styrene composites fabricated by fused deposition modeling". *Compos. Part B*, Vol. 137, pp. 51–59. doi:http://dx.doi.org/10.1016/j.compositesb.2017.11.018.